Elevating Supercapacitor Performance in Cadmium doped nickel Ferrite Nanoparticles as a Promising Innovation

S.B. Sreeja Lekshmi [a,e], S.R. Gibin [b,e], V.K. Premkumar [c], Rajeevgandhi [d]

[a]Reg.No:20113082132011, Research Scholar, Department of Physics and Research Centre, Malankara Catholic College, Mariagiri, Kaliyakkavilai-629153, Tamilnadu, India.

[b]Assistant Professor, Department of Physics and Research Centre, Malankara Catholic College, Mariagiri, Kaliyakkavilai-629153, Tamil Nadu, India.

[c]Post Doctoral Fellow Laboratory of Electrochemical Energy Storage, Institute of Environmental Resources Engineering, Zhejiang University, China.

[d]Department of Physics, Sri Indu College of Engineering and Technology, Ibrahimpatan, Telangana-501510, India.

[e]Affiliated to Manonmaniam Sundaranar University, Abishekapatti-627012, Tirunelveli, Tamil Nadu, India.

Abstract

Supercapacitors boast an extended cycle life, making them a reliable and durable energy storage solution. These compelling characteristics have spurred extensive research and exploration in the field, with the aim of developing advanced supercapacitors for various practical applications across multiple industries. In this work, $Ni_{0.5}Cd_{0.5}Fe_2O_4$ ferrite nanoparticles were successfully employed using a straightforward co-precipitation technique. The samples underwent structural and morphological characterization at different annealing temperatures (400℃, 600℃, and 700℃). X-ray diffraction analysis revealed the formation of a cubic crystal structure with a preferential orientation along the (311) plane. Through TG/DT analysis, the optimal annealing temperature was determined to be 700℃, which prompted further examination of the sample annealed at this temperature. Morphological studies using SEM and HR-TEM showed well-defined nanostructures with agglomerated spherical morphology. FTIR spectroscopy indicated an absorption range of 400 to 4000cm^{-1} for both organic and inorganic materials. The nanoparticles' surface area was measured using the BET technique, and XPS analysis identified the elemental composition and chemical states of the constituent elements. In terms of application potential, the CV study for the sample $Ni_{0.5}Cd_{0.5}Fe_2O_4$ annealed at 700 °C demonstrated a high specific capacitance of 347 Fg^{-1} at a low scan rate of 2 mVs^{-1}, highlighting its suitability for use in supercapacitors.

Graphical abstract

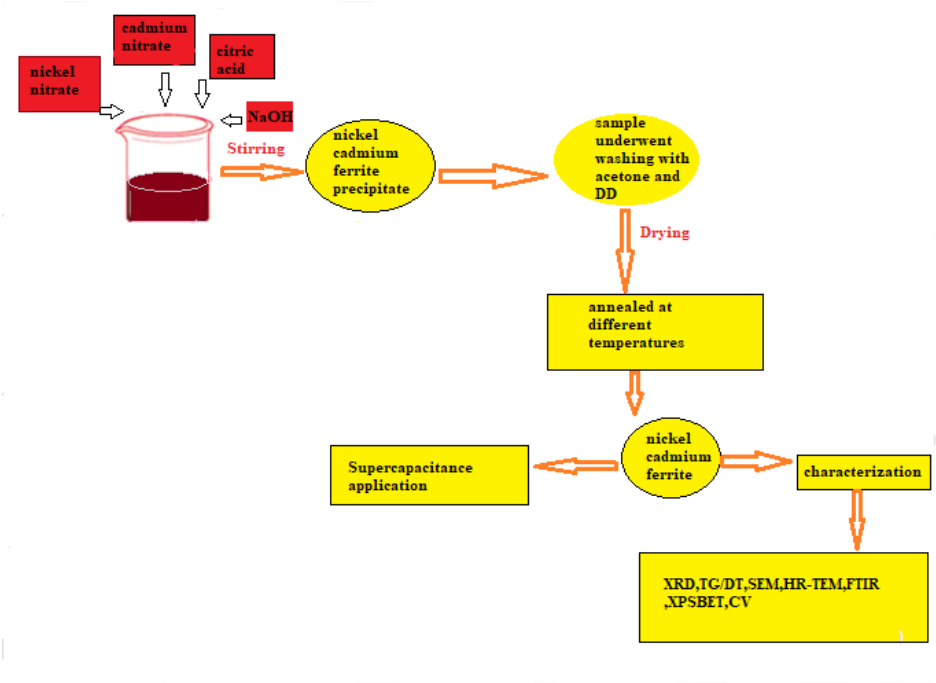

Keywords:
Supercapacitors, Co-precipitation, Cyclic voltammetry, cubic structure

Corresponding author at:
Dr. S.R. Gibin
Department of Physics and Research Centre, Malankara Catholic College, Mariagiri, Kaliyakkavilai-629153, Tamilnadu, India.
E-mail:gibin.physics@gmail.com

1. Introduction

Advancements in miniaturizing technology have rapidly propelled the development of devices such as memory, spintronics, and multifunctional gadgets [1]. These advancements have opened up a wide range of technological applications in fields like magnetic information storage, ferrofluids, magnetic-guided drug delivery, sensors, catalysts, and magnetic resonance imaging (MRI) enhancement [2-4].In recent years, there has been significant interest in supercapacitors as a novel energy storage solution due to their exceptional characteristics, including long cycle life, insensitivity to temperature fluctuations, high power density, and efficient charging and discharging capabilities.[5] Consequently, the search for new materials that can serve as potential supercapacitor electrodes has become essential to meet the demands of high power density and long-term durability in the field of energy storage. Supercapacitors can be categorized into electrochemical capacitors, which store energy through double-layer capacitance at the electrode-electrolyte interface, and pseudocapacitors, which rely on reversible faradaic redox reactions for energy storage [6-7].

Until now, researchers have investigated a wide range of materials as potential electrodes for SuperCapacitor applications [8,10]. Notably, among these materials, faradaic active SuperCapacitor materials like transition metal oxides (Co_3O_4, NiO, MnO_2, Fe_2O_3) have demonstrated remarkable specific capacitance and excellent reversibility. Some of these oxides have been combined with carbon to create metal oxide/carbon composites, resulting in significantly enhanced electrochemical properties [9]. Moreover, spinel ferrites such as MFe_2O_4 (where M = Fe, Cu, Ni, Co, etc.) and related nanocomposites have gained attention as promising materials for both Li-ion

batteries and Supercapacitor applications [11]. These materials exhibit favorable characteristics that make them potential candidates for efficient energy storage.

Magnetic nanoparticles, specifically ferrites like nickel ferrite ($NiFe_2O_4$), undergo significant changes in their properties when reduced to the nanometric range [12-14]. These changes include higher magnetic saturation, lower coercivity, increased magnetization, and reduced magnetic loss. Nickel ferrite is a multifaceted and technologically important soft ferrite material due to its typical ferrimagnetic properties, low eddy current losses, low conductivity, and high electrochemical stability. Doping ferrites with different elements in varying proportions allow for the desirable tuning of their properties [14-17]. Ni-Cd ferrite is a versatile technological material known for its intriguing magnetic and electromagnetic properties. For optimal performance in various applications, it is essential to obtain highly pure, ultrafine, and uniform particles [18]. These specific particle characteristics play a vital role in enhancing the material's capabilities and effectiveness [18]. Various methods can be used to synthesize $NiCdFe_2O_4$, with co-precipitation standing out as an advantageous option due to its quicker response times and milder reaction conditions. Compared to other techniques, co-precipitation offers a quick and cost-effective approach to producing nickel ferrite nanoparticles [19-20]. These highly pure, ultrafine, and uniform particles are crucial for achieving high performance in ferrite-based applications. Overall, nickel-cadmium ferrite exhibits fascinating magnetic and electromagnetic properties, making it a versatile material for numerous technological purposes. The main focus of this research is on the synthesis and characterization of manganese-doped nickel ferrite nanoparticles with the composition $Ni_{0.5}Cd_{0.5}Fe_2O_4$. The nanoparticles were successfully prepared using a novel co-precipitation method. The next step involved annealing the samples at varying temperatures: 400°C, 600°C, and 700°C. Subsequently, a thorough set of characterization studies was conducted to investigate the morphological and electronic properties of the synthesized samples.

The research utilized several analytical techniques, including XRD, TG/DTA, SEM, HR-TEM, FTIR, CV, XPS, and BET analysis. These investigations aimed to reveal more about the physical and chemical properties of the samples at different annealing temperatures. The ultimate goal was to understand how the annealing process affects the nanoparticles and to explore potential applications based on their unique properties.

2. Experimental studies

A novel co-precipitation technique was utilized to create nanocrystalline $Ni_{1-x}Cd_xFe_2O_4$ (x=0.5) nanoparticles, using high-purity chemicals from Merck Chemicals. The precursors, namely $Cd(NO_3)_2.4H_2O$, $Ni(NO_3)_3.6H_2O$, $Fe(NO_3)_3.9H_2O$, and citric acid ($C_6H_8O_7$), were dissolved in 20 ml of deionized water (DD), combined with 0.29 M citric acid and 4 M NaOH. Following the dissolution, the metal nitrates were mixed in a 1:2:3 molar ratio. Subsequently, a 4M NaOH solution was added as the precipitating agent, and the solution was stirred at 750 rpm at 80℃ until it reached a pH of approximately 9. The stirring was maintained for three hours at 80°C, resulting in the formation of a dark brown precipitate containing the $NiCdFe_2O_4$ nanoparticles. The dark brown precipitate underwent washing with acetone and deionized water to yield a clear precipitate. Finally, the obtained $NiCdFe_2O_4$ powder was dried using a heating mantle for 2 hours at 90-100°C, followed by annealing at different temperatures, such as 400°C, 600°C, and 700°C.

X-ray Diffraction (XRD) was employed by the researchers to determine the crystalline phase of the Cd-doped $NiFe_2O_4$ nanoparticles. The XRD analysis was conducted using a BRUKER USA D8 Advance, Davinci device, which utilized CuKα radiation with a wavelength (λ) of 1.54060 Å. The XRD instrument operated at 40kV and 30mA. Scanning of the samples was performed over a 2θ range from 20° to 80°, with a scan speed set at $10°min^{-1}$. The mean crystal diameter was estimated using the Debye Scherer formulation.

$$D = \frac{K\lambda}{(\beta \cos\theta)}$$

Here, D stands for the average crystal diameter, K is the constant (k=0.9) associated with crystal shape, λ denotes the X-ray wavelength, β is the Full width at half-maximum FWHM of the diffractionpeak, and θ is the Bragg angle.

The phase of the sample was determined using the JCPDS database, which is the Joint Committee of Powder Diffraction Standards. To evaluate the degradation performance of the prepared sample a TG/DT analysis was led using a NETZSCH-STA 449 F3 JUPITER analyzer. Elemental imaging analysis was performed using an EVO 18 model Scanning Electron Microscope (SEM) after sputtering the samples. The morphology and size of the samples were studied using HR-TEM analysis with an FEI-TECNAI G2-20 TWIN model operating at 200 kV. Elemental analysis was carried out using EDX with a Bruker EDX instrument featuring an LN2-free detector. The material was scattered across a copper grid that was coated with carbon to produce SAED patterns. XPS measurements were performed using the ULVAC-PHI MODEL: PHI5000 Version Probe 111. FTIR analysis was conducted using a Spectrum Two model. The Brunauer-Emmett-Teller (BET) method was used by Quantachrome Instruments' Autosorb IQ series to calculate the specific surface area of the nanoparticles. Utilizing the Versa STAT MC model, cyclic voltammetry (CV) was used to examine the electrochemical characteristics of the nanoparticles.

3. Result and Discussion

3.1 X-ray Diffraction

In this investigation, Nickel Cadmium Ferrite ($Ni_{0.5}Cd_{0.5}Fe_2O_4$) nanoparticle samples were subjected to X-ray diffraction (XRD) analysis at various annealing temperatures (400ºC, 600ºC, 700ºC). The XRD pattern (Fig.1) exhibited distinct and well-defined diffraction peaks at specific 2θ values, corresponding to particular crystallographic planes. The identified planes and their respective 2θ values were as follows: (220) at 30°, (311) at 35°, (222) at 35.8°, (400) at 40°, (511) at 59.7°, (440) at 62.8°, (422) at 52.9° and (533) at 74°. These patterns were in excellent agreement with reference data from the JCPDS database (card no 22-1063 and card no 10-0325), confirming the presence of a sharp and intense diffraction pattern [21-25]. The analysis revealed a single cubic phase with an fcc structure for $Ni_{0.5}Cd_{0.5}Fe_2O_4$, indicating the absence of impurity phases [21]. The lack of ambiguous reflections, apart from the spinel structures, underscored the homogeneity of the prepared samples [26].

To determine the crystallite size of the nanoparticles, the Debye Scherrer formula was applied, utilizing the XRD peak's full width at half maximum (FWHM) in radians (β), the Bragg angle (θ), and the X-ray wavelength (λ = 1.5405 A for Cu-Kα radiation) [24]. Based on the calculations, the average crystalline size was determined to be 28 nm [21]. These findings offer valuable insights into the structural characteristics and uniformity of the $Ni_{0.5}Cd_{0.5}Fe_2O_4$nanoparticle samples, contributing to a deeper understanding of their crystallographic properties.

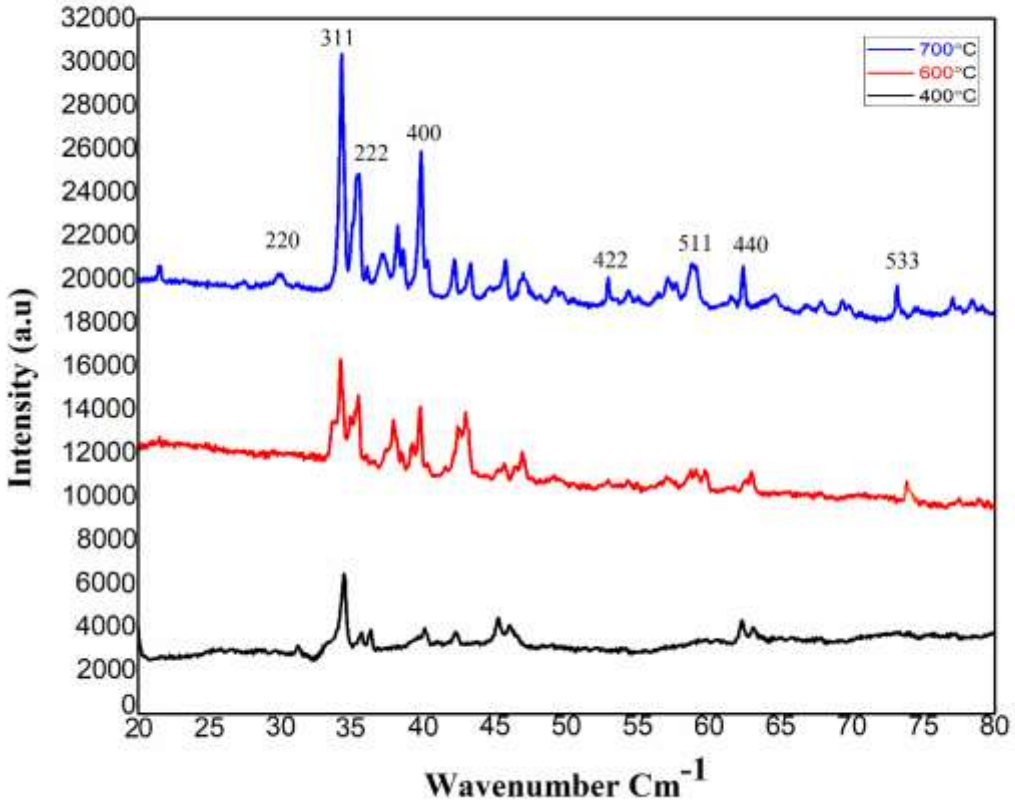

Fig .1. XRD images of $Ni_{0.5}Cd_{0.5}Fe_2O_4$ at 400℃,600℃,700℃

3.2 Thermogravimetric Analysis

Thermal analysis using TG-DTA was conducted to investigate the characteristics of nickel-cadmium ferrite, which is depicted in (Fig.2). The results revealed distinct stages of weight loss and corresponding thermal peaks. Initially, up to 105℃, a 5% weight loss occurred due to the evaporation of water molecules, accompanied by a minor endothermic peak at 100°C, likely due to the heat absorption required for water decomposition [27]. In the subsequent step, up to 470℃, a 3% weight loss and an exothermic peak at 220℃ in the DTA curve indicated the decomposition of nitrate into metal oxides [28]. The third step, up to 650°C, showed a 1% weight loss, a small endothermic peak, and a broad exothermic peak between 520℃ and 670℃, indicating the release of energy involved in phase formation.

At around 675℃, the exothermic reaction pointed to the formation of $Ni_{0.5}Cd_{0.5}Fe_2O_4$, confirming the synthesis of the desired ferrite [29]. Beyond this temperature, no significant thermal effects were observed in the DTA, signifying the stability of th**e** $Ni_{0.5}Cd_{0.5}Fe_2O_4$ phase.

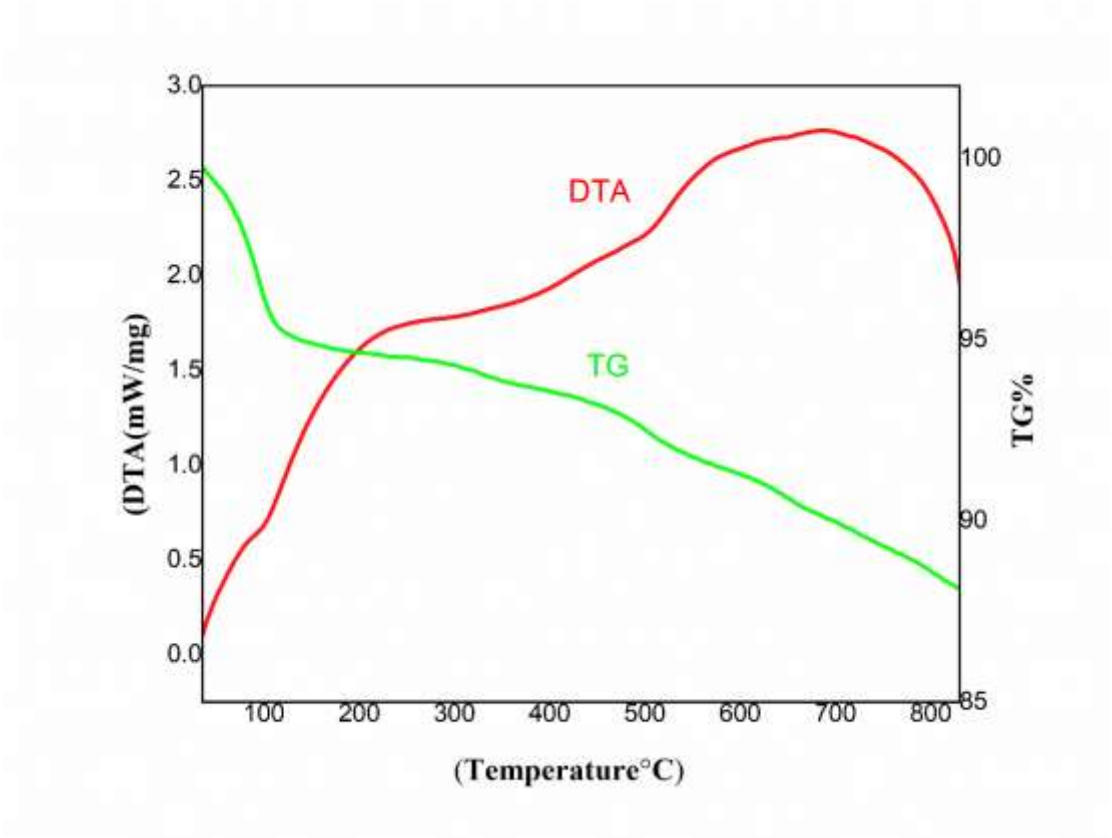

Fig.2. TG/DT analysis of $Ni_{0.5}Cd_{0.5}Fe_2O_4$ at 700℃

3.3 Fourier-Transform Infrared Spectroscopy

The FTIR spectrum of pure $Ni_{0.5}Cd_{0.5}Fe_2O_4$, which underwent calcination at 700℃ and is represented in (Fig.3). An extensive absorption band centered at 3418 cm^{-1} is attributed to the stretching vibrations of -OH groups. This indicates the presence of water molecules coordinated with the ferrite structure. This broad absorption band could arise from either atmospheric water molecules or OH groups. This observation has also been reported earlier by G.n chaudheri [30]. A minor absorption band at 2465cm^{-1} is observed, and it is attributed to adsorbed or atmospheric CO_2. The most prominent band, situated at approximately 641 cm-1 (υ_1), corresponds to the intrinsic stretching vibrations of Cd^{2+} ions and oxygen at the tetrahedral A-site in the crystal structure. On the other hand, the least intense band, around 466 cm^{-1} (υ_2), is associated with the stretching vibrations of Fe^{3+} and Ni^{3+} ions in the octahedral B-site of the crystal structure [31-32]. Furthermore, absorption bands observed at ~900 – 1000 and 1649 cm-1 are assigned to the C-H group and C-O stretching vibrations, respectively [31].

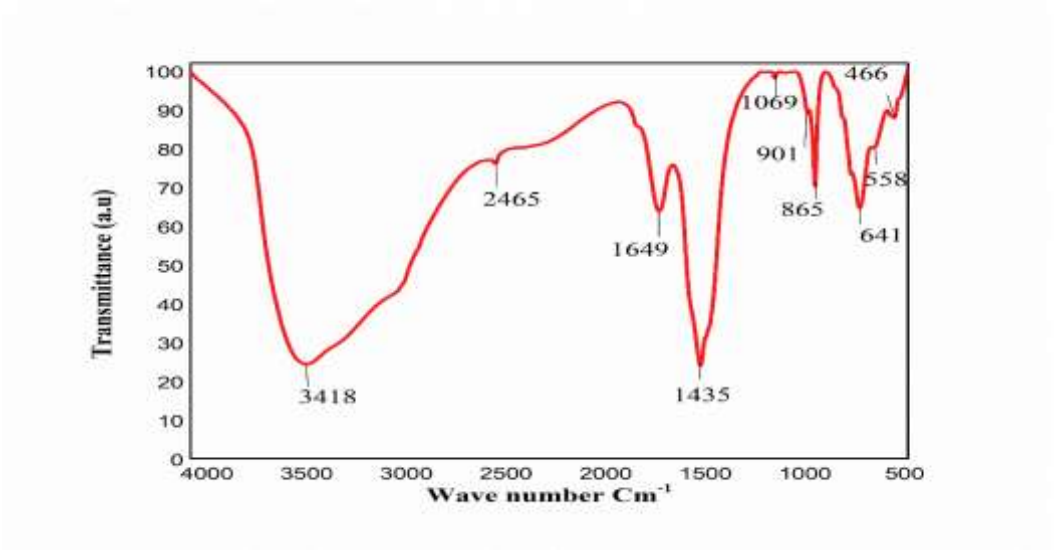

Fig.3. FTIR Spectrum of $Ni_{0.5}Cd_{0.5}Fe_2O_4$ sample

3.4 Scanning electron microscope

After annealing the $Ni_{0.5}Cd_{0.5}Fe_2O_4$ sample at 700℃, its surface morphology was examined using SEM (Fig.4 (a, b,c)). The SEM images revealed the presence of spherical particles with some agglomeration, indicating that certain particles had clustered together. Additionally, evidence of intergranular diffusion was observed, suggesting that atomic or molecular diffusion occurred between adjacent particles at the grain boundaries. The agglomeration of particles was attributed to the interaction between magnetic particles and the high surface energy of the nanocomposites. This SEM analysis provides valuable insights into the microstructure of the annealed sample, which may influence its magnetic properties and overall behavior [33]. Further characterization techniques, such as X-ray diffraction (XRD) and Transmission Electron Microscopy (HR-TEM), could be employed to complement and deepen the understanding of the material's properties.

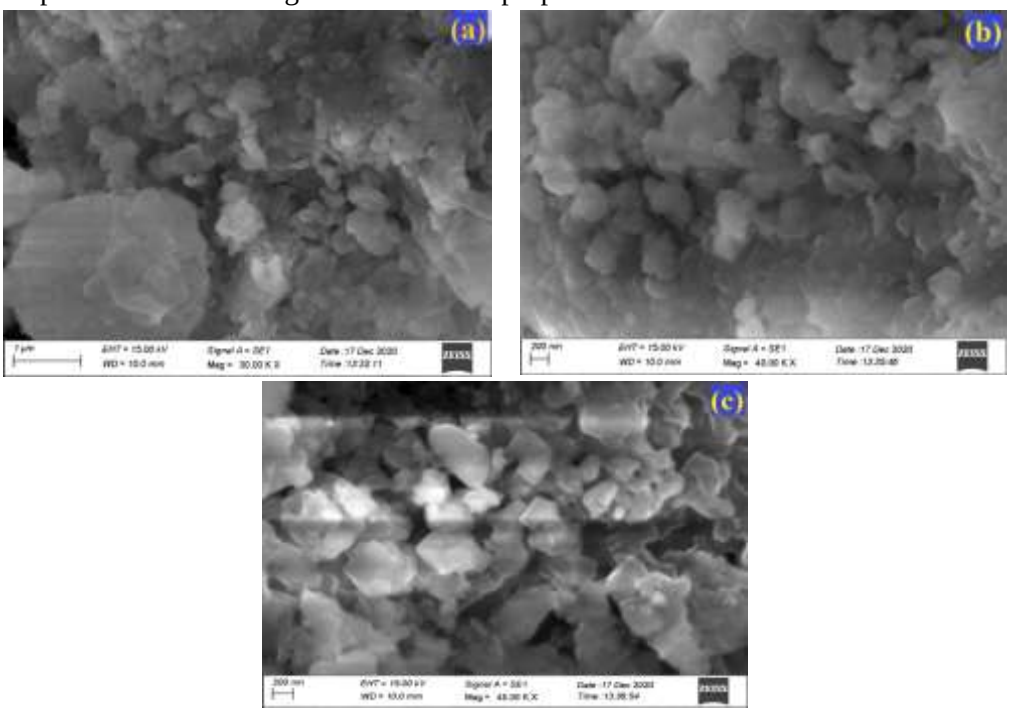

Fig.4. (a,b,c) SEM images of $Ni_{0.5}Cd_{0.5}Fe_2O_4$ at 700℃

3.5 High–resolution transmission electron microscope

In this study, $Ni_{0.5}Cd_{0.5}Fe_2O_4$ nanoparticles were thoroughly characterized using HR-TEM which depicts in Fig.5 (a,b,c,d). The average particle size, determined through the 'j' viewer software and presented in Fig.5(e) was found to be around 37 nm [33-34]. The HR-TEM analysis revealed that the nanoparticles exhibited a roughly spherical shape with slight agglomeration, likely due to magnetic dipole-dipole interactions among the particles. These results align with an earlier report by Monica Sani *et al.*, [34]. This outcome is consistent with the findings obtained from X-ray diffraction (XRD) analysis Additionally, the SAED pattern showed well-defined and separate continuous rings, indicating the nanoparticles' well-crystalline nature.

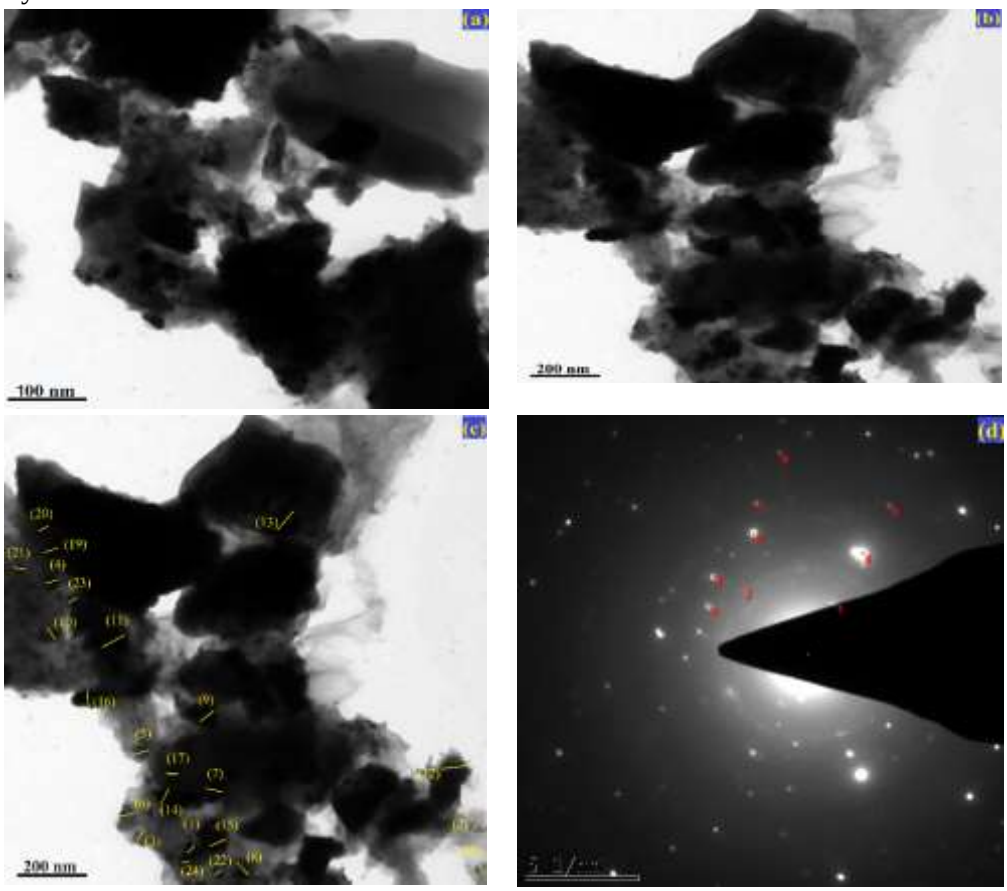

Fig.5. (a,b,c,d) HR-TEM images of $Ni_{0.5}Cd_{0.5}Fe_2O_4$ at 700℃

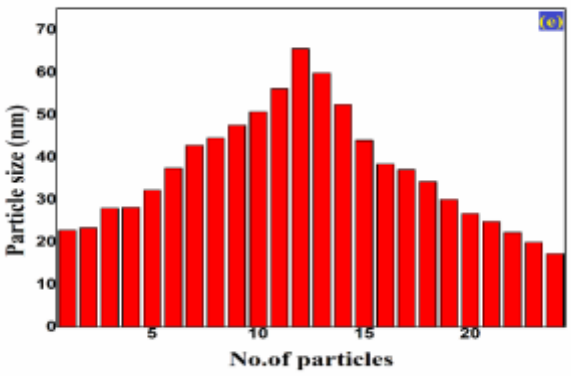

Fig.5. (e) Average particle size using image 'j' viewer software from HR-TEM

No. of. particles	Particle size(nm)	No.of .particles	Particle size(nm)
1	22.764	14	52.388
2	23.294	15	43.962
3	27.935	16	38.331
4	28.152	17	37.037
5	32.194	18	34.208
6	37.365	19	30.038
7	42.751	20	26.708
8	44.513	21	24.815
9	47.495	22	22.222
10	50.608	23	19.907
11	56.103	24	17.201
12	65.554	average	36.9
13	59.812		

Table 1. No. of particles and particle size $Ni_{0.5}Cd_{0.5}Fe_2O_4$ using image 'j' viewer software from HR-TEM.

3.6 Energy Dispersive X-ray Spectroscopy

The Energy Dispersive X-ray Spectroscopy (EDX) spectrum displayed in Fig.6 reveals the presence of Nickel (Ni), Cadmium (Cd), Iron (Fe), and Oxygen (O) elements in the $Ni_{0.5}Cd_{0.5}Fe_2O_4$ ferrite samples. The absence of any additional peaks in EDX spectra provides strong evidence that the ferrite samples are free from impurities or foreign elements, thus confirming their high purity. This assurance is crucial for accurately studying and utilizing the material's specific properties, which rely on its elemental composition without interference from contaminants.

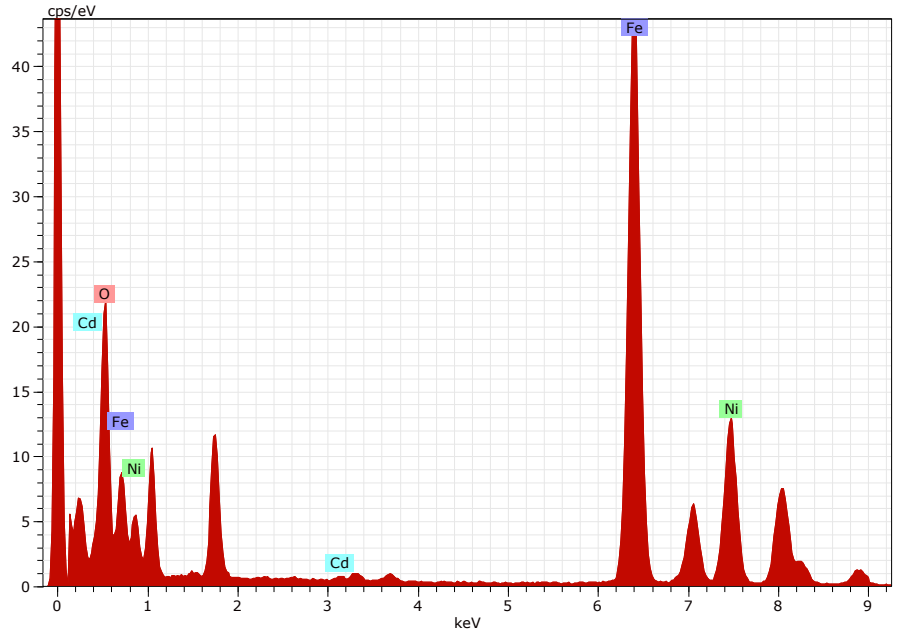

Fig.6.EDX analysis of the sample $Ni_{0.5}Cd_{0.5}Fe_2O_4$ (x=0.5) at 700℃

Element	**Series**	**Net**	**unn.C [wt.%]**	**norm.C [wt.%]**	**Atom. C [at.%]**	**Error (3 Sigma)**
Oxygen	K-series	19422	19.34	19.34	46.06	1.86
Nickel	K-series	24688	19.63	19.63	12.75	1.89
Iron	K-series	82939	59.73	59.73	40.76	5.49
Cadmium	K-series	102	1.30	1.30	0.44	0.51

Table.2 Elemental compositions of $Ni_{0.5}Cd_{0.5}Fe_2O_4$

3.7 X-ray photoelectron spectroscopy

XPS analysis is an important method to identify quantitatively determine the surface components and composites of the sample. The wide scan XPS spectra of the sample in the binding energy range(0–1000eV) are shown in Fig.7e. The individual components of the composites were confirmed by individual XPS Spectra of Oxygen (O1s), Ferrite (Fe2p), Nickel (Ni2p), Cadmium (Cd3d) and $NiCdFe_2O_4$ as shown in Fig. 7(a-e) respectively.

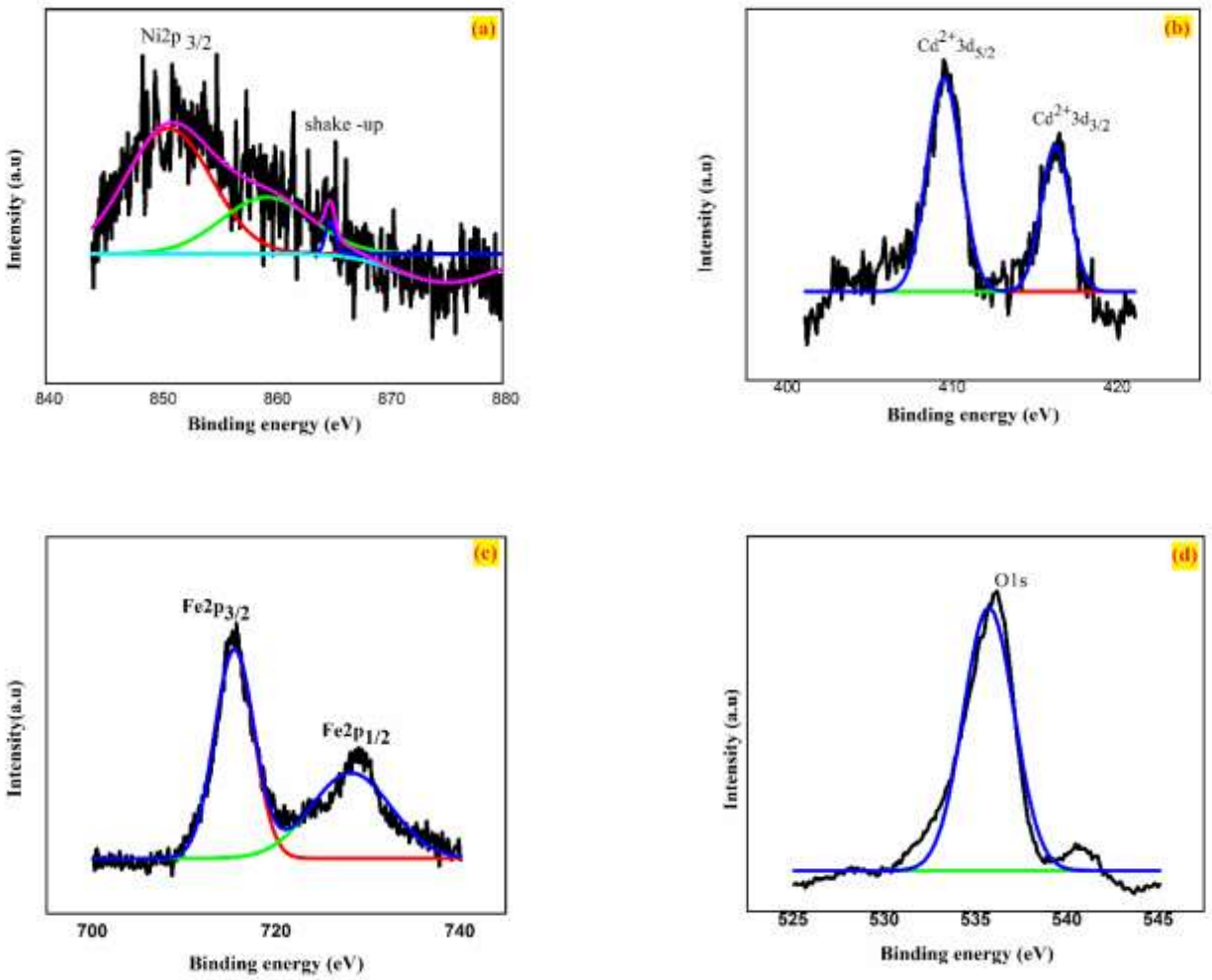

Fig.7(a-d) XPS spectrum of Ni2p,Cd3p,Fe2p,O1s of $Ni_{0.5}Cd_{0.5}Fe_2O_4$ sample.

The wide scan XPS spectra of the sample are given in Fig.7e The binding energies of the individual components O1s, Fe2p, Ni2p, and Cd3d were tabulated in Table 3. The binding energies of Ni2p and Ni 2p1 for the sample were obtained, respectively as 854.97 eV and 878.08 eV (Fig.7a and Table 3). The value of FWHM for each spin–orbit component is the same, but for Ni2p the Ni2p1 component is much broader than the Fe2p peak. It is caused by the coaster–kroning effect (post–ionization) Ni 2p1 peak is much shorter compared to Fe_2p3/2. XPS spectra of cadmium, there are two peaks in the binding energy region Cd3d3/2 and Cd3d5/2 were observed,

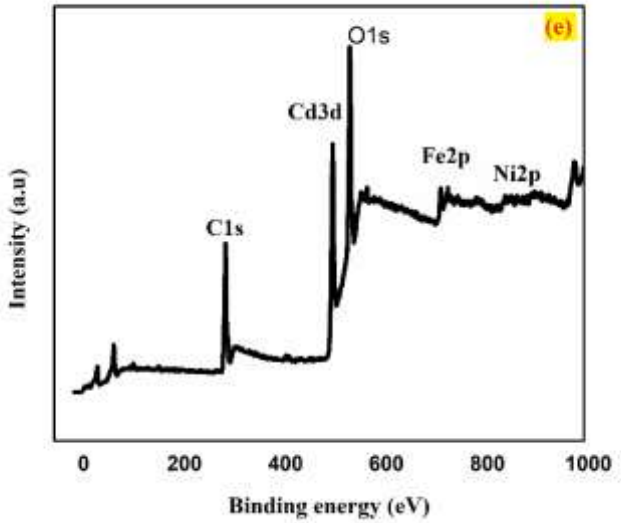

Fig .7e Wide spectrum of $Ni_{0.5}Cd_{0.5}Fe_2O_4$ sample.

Where the peaks ((Cd 3d3/2), 409.86 eV) and peaks ((Cd 3d5/2) 417.05 eV) correspond well with the values in the literature (Fig.7b and Table 3). XPS results also reveal and confirm the presence of Fe^{2+}, $Ni^{2+,}$ and Cd^{3+} on the surface of the sample Cd doped $NiFe_2O_4$ sample [36-37].

Name of Elements	Peak BE	FWHM eV	Area (P) CPS.eV
O1s	536.08	4.01	577848.39
Fe2p	716.14	5.08	138224.13
Cd 3d3/2	409.86	3.99	25248.45
Cd 3d5/2	417.05	2.38	47963.67
C1s	289.86	2.57	37943.48
O1s	535.97	3.21	70131.20
Fe2p	715.36	4.84	20310.22
Ni2p	854.97	0.19	4419.61
Ni2p1	878.08	1.03	13032.45

Table .3 Elements and peak values for $Ni_{0.}Cd_{0.5}Fe_2O_4$

3.8 Brunauer-Emmett Teller

In order to investigate $Ni_{0.5}Cd_{0.5}Fe_2O_4$ nanoparticles, Brunauer-Emmett-Teller (BET) measurements have been used. Fig.8a illustrates the 0.0–1.0 relative pressure region, which is close to the Type IV curve, N2 isotherms show an obvious hysteresis loop [38]. Based on N2 isotherms, the BET-specific surface area of the synthesized $Ni_{0.5}Cd_{0.5}Fe_2O_4$ was 19.528 m^2g^{-1}. The interparticle gaps and the mesoporous structure of the $Ni_{0.5}Cd_{0.5}Fe_2O_4$ nanoparticles were shown by the Barrett-Joyner-Halenda (BJH) method to account for the pore diameter of 3.35 nm. The large specific surface area of the Nickel-cadmium Ferrite

nanoparticles may be due to the tiny sample size. In comparison to the previous report, a $Ni_{0.5}Cd_{0.5}Fe_2O_4$ with a higher specific surface area may provide more efficient active sites, increasing the electrochemical performance of the supercapacitors [38].

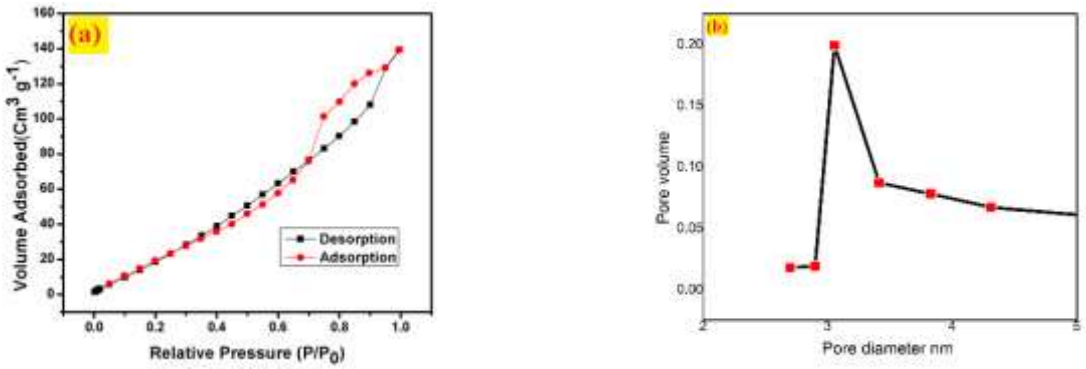

Fig.8. N_2-adsorbtion–desorption isotherms. b) Pore size distribution curve of $Ni_{10.5}Cd_{0.5}Fe_2O_4$.

3.9 Cyclic voltammetry

In this study, the electrochemical properties of $Ni_{0.5}Cd_{0.5}Fe_2O_4$ electrodes were thoroughly investigated. Upon analysis of the data, it was observed that the specific capacitance values exhibited a decreasing trend as the scan rate increased. The trends are visually represented in Fig.9 and Table 4 consist of cyclic voltammeter (CV) curves recorded at different scan rates, ranging from 2 mVs^{-1} to 10 mVs^{-1}. Notably, the study revealed that the specific capacitance is maximized when a low scan rate is employed. The reason behind the higher specific capacitance at lower scan rates may be linked to the limited occurrence of faradaic reactions. At higher scan rates, ionic diffusion predominantly happens from the outer regions of the pores, resulting in reduced involvement of the interior surfaces. Conversely, lower scan rates involve both interior and outer surfaces, leading to a higher specific capacitance.

The electrochemical measurement revealed that $Ni_{0.5}Cd_{0.5}Fe_2O_4$ annealed at 700℃ demonstrated the highest specific capacitance of 347 Fg^{-1} at the lowest scan rate of 2 mVs^{-1}. However, at a higher scan rate of 10 mVs^{-1}, the specific capacitance decreased significantly to 53 Fg^{-1}.In comparison to a previous study by Rajeevegandhi *et al;* [33], which reported a maximum specific capacitance of 338 Fg^{-1} for $Cd_{0.3}Ni_{0.7}Fe_2O_4$ nanoparticles annealed at 600 °C, the present study exhibited notably higher specific capacitance for $Ni_{0.5}Cd_{0.5}Fe_2O_4$ annealed at 700℃. The improved crystallinity of the $Ni_{0.5}Cd_{0.5}Fe_2O_4$ nanoparticles observed in this investigation contributed to the higher specific capacitance values obtained, enhancing the overall electrochemical performance.

In comparison, Ankur Soam *et al;* [35] reported a specific capacitance value of 207 Fg^{-1} for $NiFe_2O_4$ at a scan rate of 5 mVs^{-1}, this study demonstrates that substituting Cadmium in Nickel spinel ferrites ($Ni_{0.5}Cd_{0.5}Fe_2O_4$) nanoparticles leads to improved overall electrochemical performance. The specific capacitance values obtained for $Ni_{0.5}Cd_{0.5}Fe_2O_4$, particularly at the lowest scan rate of 2 mVs^{-1} (347 Fg^{-1}), significantly surpassed those of pure

$NiFe_2O_4$, indicating the beneficial effect of incorporating Cadmium on the material's electrochemical properties.

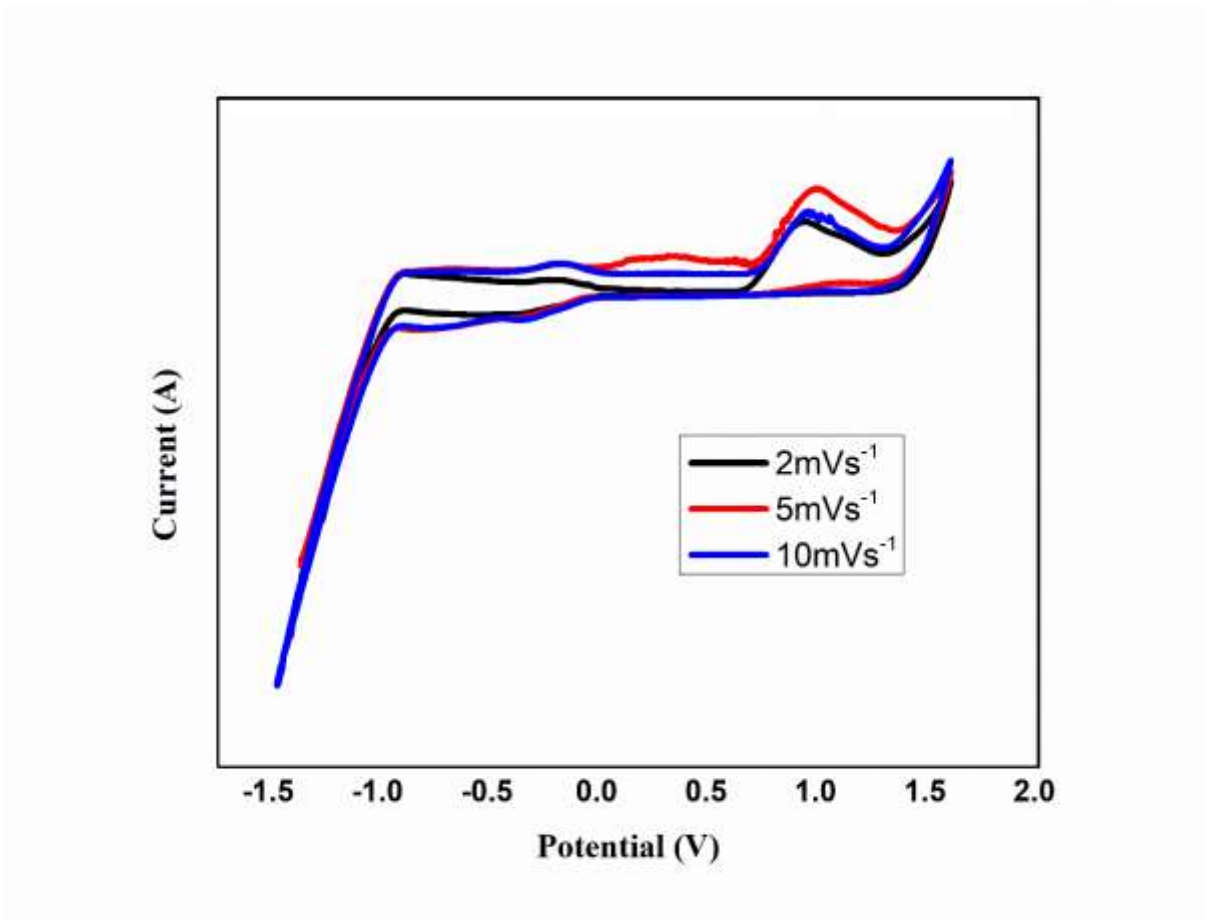

Fig.9. CV curves of the sample $Ni_{0.5}Cd_{0.5}Fe_2O_4$ at the scan rate of $2mVs^{-1}$, $5mVs^{-1}$, $10mVs^{-1}$

Scan rate (mVs^{-1})	Specific capacitance (Fg^{-1})
2	347
5	271
10	53

Table.4 The specific Capacitance value of $Ni_{0.5}Cd_{0.5}Fe_2O_4$ (700 ºC) for different scan rates

Conclusion

The study delved into the production and examination of nanocomposites composed of nickel-cadmium ferrite ($Ni_{0.5}Cd_{0.5}Fe_2O_4$), prepared via a chemical co-precipitation technique. X-ray diffraction (XRD) analysis consistently revealed a cubic phase indicative of $Ni_{0.5}Cd_{0.5}Fe_2O_4$ nanocomposites across all samples, irrespective of their concentrations or the annealing process. This discovery provides valuable insights into the material's structural characteristics. Fourier-transform infrared spectroscopy (FTIR) confirmed the presence of stretching vibrations at both tetrahedral and octahedral sites within the nanocomposites. This outcome aids in understanding the material's chemical makeup and bonding patterns.

HRTEM provides a powerful means of scrutinizing the nanoscale structure and morphology of materials. Electrochemical measurements showcased a noteworthy enhancement in the specific capacitance of the nickel-cadmium ferrite electrode material, particularly at lower scan rates. This suggests that the developed nanocomposites hold significant potential as electrode materials for electrochemical capacitors. Specific capacitance serves as a pivotal metric for assessing material suitability in energy storage applications. These findings have the potential to contribute significantly to the advancement of efficient energy storage materials for a wide array of applications.

Reference

[1] Kardile, H.J., Somvanshi, S.B., Chavan, A.R., Pandit, A.A. and Jadhav, K.M., 2020. Effect of Cd^{2+} doping on structural, morphological, optical, magnetic and wettability properties of nickel ferrite thin films. *Optik*, *207*, p.164462.

[2] Bharati, V.A., Somvanshi, S.B., Humbe, A.V., Murumkar, V.D., Sondur, V.V. and Jadhav, K.M., 2020. Influence of trivalent Al–Cr co-substitution on the structural, morphological and Mössbauer properties of nickel ferrite nanoparticles. *Journal of Alloys and Compounds*, *821*, p.153501.

[3] Valenzuela, R., 2012. Novel applications of ferrites. *Physics Research International*, *2012*.

[4] Vignesh, V., Subramani, K., Sathish, M. and Navamathavan, R., 2018. Electrochemical investigation of manganese ferrites prepared via a facile synthesis route for supercapacitor applications. *Colloids and Surfaces A: Physicochemical and Engineering Aspects*, *538*, pp.668-677.

[5] Dhas, S.D., Maldar, P.S., Patil, M.D., Nagare, A.B., Waikar, M.R., Sonkawade, R.G. and Moholkar, A.V., 2020. Synthesis of NiO nanoparticles for supercapacitor application as an efficient electrode material. *Vacuum*, *181*, p.109646.

[6] Bhujun, B., Tan, M.T. and Shanmugam, A.S., 2017. Study of mixed ternary transition metal ferrites as potential electrodes for supercapacitor applications. *Results in Physics*, *7*, pp.345-353.

[7] Soam, A., Kumar, R., Thatoi, D. and Singh, M., 2020. Electrochemical performance and working voltage optimization of nickel ferrite/graphene composite based supercapacitor. *Journal of Inorganic and Organometallic Polymers and Materials*, *30*, pp.3325-3331.

[8] Kennaz, H., Harat, A., Guellati, O., Momodu, D.Y., Barzegar, F., Dangbegnon, J.K., Manyala, N. and Guerioune, M., 2018. Synthesis and electrochemical investigation of spinel cobalt ferrite magnetic nanoparticles for supercapacitor application. *Journal of Solid State Electrochemistry*, *22*, pp.835-847.

[9] Zhu, M., Wang, Y., Meng, D., Qin, X. and Diao, G., 2012. Hydrothermal synthesis of hematite nanoparticles and their electrochemical properties. *The Journal of Physical Chemistry C*, *116*(30), pp.16276-16285.

[10] Lee, S.W., Kim, B.S., Chen, S., Shao-Horn, Y. and Hammond, P.T., 2009. Layer-by-layer assembly of all carbon nanotube ultrathin films for electrochemical applications. *Journal of the American Chemical Society*, *131*(2), pp.671-679.

[11] Kumbhar, V.S., Jagadale, A.D., Shinde, N.M. and Lokhande, C.D., 2012. Chemical synthesis of spinel cobalt ferrite ($CoFe_2O_4$) nano-flakes for supercapacitor application. *Applied Surface Science*, *259*, pp.39-43.

[12] Maaz, K., Karim, S., Mumtaz, A., Hasanain, S.K., Liu, J. and Duan, J.L., 2009. Synthesis and magnetic characterization of nickel ferrite nanoparticles prepared by co-precipitation route. *Journal of Magnetism and Magnetic Materials*, *321*(12), pp.1838-1842.

[13] Kumar, G.R., Kumar, K.V. and Venudhar, Y.C., 2012. Synthesis, structural and magnetic properties of copper substituted nickel ferrites by sol-gel method.

[14] Sagadevan, S., Chowdhury, Z.Z. and Rafique, R.F., 2018. Preparation and characterization of nickel ferrite nanoparticles via co-precipitation method. *Materials Research*, *21*.

[15] Vinosha, P.A., Xavier, B., Ashwini, A., Mely, L.A. and Das, S.J., 2017. Tailoring the photo-Fenton activity of nickel ferrite nanoparticles synthesized by low-temperature coprecipitation technique. *Optik*, *137*, pp.244-253.

[16] Nordblad, P., Mohan, R. and Mukherjee, S., 2017. Structural, magnetic and hyperfine characterizations of nanocrystalline Zn-Cd doped nickel ferrites. *Journal of Magnetism and Magnetic Materials*, *441*, pp.710-717.

[17] Ali, N.J., Rahman, J. and Chowdhury, M.A., 2000. The influence of the addition of CaO on the magnetic and electrical properties of Ni–Zn ferrites. *Japanese Journal of Applied Physics*, *39*(6R), p.3378.

[18] De, M., Mukherjee, A. and Tewari, H.S., 2015. Characterization of cadmium substituted nickel ferrites prepared using auto-combustion technique. *Processing and Application of Ceramics*, *9*(4), pp.193-197.

[19] Amin, N., Hasan, M.S.U., Majeed, Z., Latif, Z., un Nabi, M.A., Mahmood, K., Ali, A., Mehmood, K., Fatima, M., Akhtar, M. and Arshad, M.I., 2020. Structural, electrical, optical and dielectric properties of yttrium substituted cadmium ferrites prepared by Co-Precipitation method. *Ceramics International*, *46*(13), pp.20798-20809.

[20] Kulkarni, A.B., Hegde, N.D., Gowda H, S. and Mathad, S.N., 2020, October. Influence of cadmium substitution on structural and mechanical properties of Co- Ni nano ferrite synthesized by co- precipitation method. In *Macromolecular Symposia* (Vol. 393, No. 1, p. 1900213).

[21] Nandanwar, A.K., Sarkar, N.N., Sahu, D.K., Choudhary, D.S. and Rewatkar, K.G., 2018. Effect of Ni^{+2} substitution on structural and electrical behaviour of nano-size cadmium ferrites. *Materials Today: Proceedings*, *5*(10), pp.22669-22674.

[22] Kharat, K.R., Jadhav, S.L., Jadhav, A.L., Kadam, A.V., Bhosale, J.L. and Magdum, T.S., 2021. Effect of Cd^{2+} Substituted Nickel Ferrite oxide ($Ni_{1-x}Cd_xFe_2O_4$) on Magnetic, Dielectric and Structural Properties.

[23] Henaish, A.M.A., El-Sharkawy, A.N., Shama, S.A., Hemeda, O.M. and Ghazy, R., 2019, June. Structure and optical properties of nano Ni_x Cd_{1-x} Fe_2O_4 doped with optical dyes. In *Journal of Physics: Conference Series* (Vol. 1253, No. 1, p. 012024). IOP Publishing.

[24] Sivakumar, P., Ramesh, R., Ramanand, A., Ponnusamy, S. and Muthamizhchelvan, C., 2011. Synthesis and characterization of nickel ferrite magnetic nanoparticles. *Materials Research Bulletin*, *46*(12), pp.2208-2211.

[25] Yattinahalli, S.S., Kapatkar, S.B., Ayachit, N.H. and Mathad, S.N., 2013. Synthesis and structural characterization of nanosized nickel ferrite. *International Journal of Self-Propagating High-Temperature Synthesis*, *22*, pp.147-150.

[26] Rahimi, M., Eshraghi, M. and Kameli, P., 2014. Structural and magnetic characterizations of Cd substituted nickel ferrite nanoparticles. Ceramics international, 40(10), pp.15569-15575.

[27] Kamble, R.B., Varade, V., Ramesh, K.P. and Prasad, V., 2015. Domain size correlated magnetic properties and electrical impedance of size dependent nickel ferrite nanoparticles. *AIP Advances*, *5*(1).

[28] Liu, X.M. and Gao, W.L., 2012. Preparation and magnetic properties of $NiFe_2O_4$ nanoparticles by modified pechini method. *Materials and Manufacturing Processes*, *27*(9), pp.905-909.

[29] Jadhav, S.P., Toksha, B.G., Jadhav, K.M. and Shinde, N.D., 2010. Effect of cadmium substitution on structural and magnetic properties of nano sized nickel ferrite. *Chinese Journal of Chemical Physics*, *23*(4), p.459.

[30] Chaudhari, G.N., 2014. AC Impedance spectroscopy study on Nickel doped Cadmium Ferrites Nano particles prepared by sol-gel citrate method. *measurements*, *3*(10).

[31] Singh, S., Hitkari, G. and Pandey, G., 2017. Synthesis and characterization of cadmium doped nickel ferrite ($Ni_{0.6}Cd_{0.4}Fe_2O_4$) nanoparticles and its optical properties. *International Journal of Scientific & Engineering Research*, *8*(5).

[32] Bakale, P., Guggari, P., Keste, A., Pujar, A.S., Mathad, S.N., Hiremath, C.S., Jeergal, P.R. and Pujar, R.B., 2019. Synthesis, structural and mechanical properties of Ni1-xCdxFe2O4 ferrites (X= 0.1, 0.2, 0.3, and 0.4). *combustion*, *20*, p.21.

[33] Rajeevgandhi, C. and Sivagurunathan, P., 2019. Essance of supercapacitor and electrical behaviour of cadmium nickel ferrite nanocomposites prepared by chemical Co-precipitation method. *Int J Adv Sci Technol*, *28*(2019), pp.431-446.

[34] Saini, M., Shukla, R. and Kumar, A., 2019. Cd^{2+} substituted nickel ferrite doped polyaniline nanocomposites as effective shield against electromagnetic radiation in X-band frequency. *Journal of Magnetism and Magnetic Materials*, *491*, p.165549.

[35] Soam, A., Kumar, R., Sahoo, P.K., Mahender, C., Kumar, B., Arya, N., Singh, M., Parida, S. and Dusane, R.O., 2019. Synthesis of nickel ferrite nanoparticles supported on graphene nanosheets as composite electrodes for high performance supercapacitor. *ChemistrySelect*, *4*(34), pp.9952-9958.

[36] Dojcinovic, M.P., Vasiljevic, Z.Z., Rakocevic, L., Pavlovic, V.P., Ammar-Merah, S., Vujancevic, J.D. and Nikolic, M.V., 2023. Humidity and Temperature Sensing of Mixed Nickel–Magnesium Spinel Ferrites. *Chemosensors*, *11*(1), p.34.

[37] Zhang, Y., Sun, A. and Suonan, Z., 2021. The structural, magnetic, and optical properties of Ni–Mg–Zn ferrite prepared with different complexing agents via sol–gel method. *Journal of Materials Science: Materials in Electronics*, *32*, pp.13350-13368.

[38] Jeseentharani, V., George, M., Jeyaraj, B., Dayalan, A. and Nagaraja, K.S., 2013. Synthesis of metal ferrite (MFe2O4, M= Co, Cu, Mg, Ni, Zn) nanoparticles as humidity sensor materials. *Journal of experimental nanoscience*, *8*(3), pp.358-370.